International Journal of Nanomedicine

Dovepress
open access to scientific and medical research

Open Access Full Text Article

ORIGINAL RESEARCH

Synergistic Photothermal Tumor Immunotherapy by 1-MT Based on Zeolitic Imidazolate Framework-8 with pH-High Sensitivity

Ruijing Su*, Yue Yang*, Haiyan Wu, Bo Liu, Xinyuan Tian, Chaoyu Zhou, Yanxin Hu, Tianlong Liu

Laboratory of Veterinary Pathology and Nanopathology, College of Veterinary Medicine, China Agricultural University, Beijing, 100193, People's Republic of China

*These authors contributed equally to this work

Correspondence: Tianlong Liu; Yanxin Hu, Email liutianlong@cau.edu.cn; huyx@cau.edu.cn

Background: A successful immune response against tumors depends on various cellular processes. Hence, there is an urgent need to construct a proficient nanoplatform for immunotherapy that can concurrently regulate the activities of various cells participating in the immune process. We have developed zeolitic imidazolate framework-8 (ZIF-8) formula, with good pH sensitivity, which is conducive to the release of drugs in the tumor site (acidic environment) and significantly improves immunotherapy. This is achieved through the coordinated action of different therapeutic agents, such as the photothermal agent polydopamine (PDA), the chemodrug camptothecin (CPT), and the immunomodulator 1-methyl-D-tryptophan (1-MT).

Materials and Methods: In this study, we evaluated the antitumor effect of PDA/(CPT + 1-MT) @ZIF-8 (PCMZ) nanoparticles (NPs) in vitro and in vivo and investigated the molecular mechanism of PCMZ NPs in tumor suppression via photothermal-chemo-immunotherapy.

Results: MTT and Annexin V-FITC/PI double staining apoptosis test showed that PCMZ NPs could induce apoptosis of 4T1 cell, and PCMZ NPs could cause 4T1 cell necrosis under 808 nm laser irradiation. The objective is to establish a unilateral breast cancer model in mice and investigate the effect of PCMZ NPs on tumor growth and tumor suppression in tumor bearing mice. The results showed that PCMZ NPs showed good heating effect in vivo and effectively inhibited tumor growth under 808 nm laser irradiation. In addition, PCMZ NPs could induce the immunogenic death of tumor cells, promote the maturation of DCs, inhibit IDO pathway, and finally differentiate T cells into cytotoxic T cells and helper T cells, so as to effectively activate the anti-tumor immune response.

Conclusion: The PCMZ NPs, possessing good photothermal conversion capabilities due to join of PDA, effectively overcome two main challenges in immunotherapy: insufficient stimulation of the immune response and evasion of the immune system. This provides a robust platform against invasive cancer and recurrent tumors.

Keywords: zeolitic imidazolate framework-8, photothermal agent polydopamine, 1-methyl-D-tryptophan, photoluminescence, camptothecin

Introduction

Over the past few years, there has been a rise in the use of antitumor immunotherapy, which involves stimulating the body's natural immune response, as a potential treatment for tumors.[1] Immunotherapy was anticipated to achieve comprehensive antitumor effects throughout the body, inhibiting abscopal tumors that are difficult to access with local treatments. Additionally, it was expected to establish robust immunological memory to combat rechallenged tumors following the eradication of primary tumors.[2] Nevertheless, the intricate antitumor immune reaction encompassed various cells, leading to the unsatisfactory outcome of clinical immunotherapy.[3,4] DCs are carried out around the immune cells.[5] During the maturation process, DCs move from the outer tissues where they come into contact with the antigen to the secondary lymphoid organs. There, they interact with T cells and trigger an immune response.[6] As the most powerful

Received: 2 April 2024
Accepted: 7 August 2024
Published: 20 August 2024

Graphical Abstract

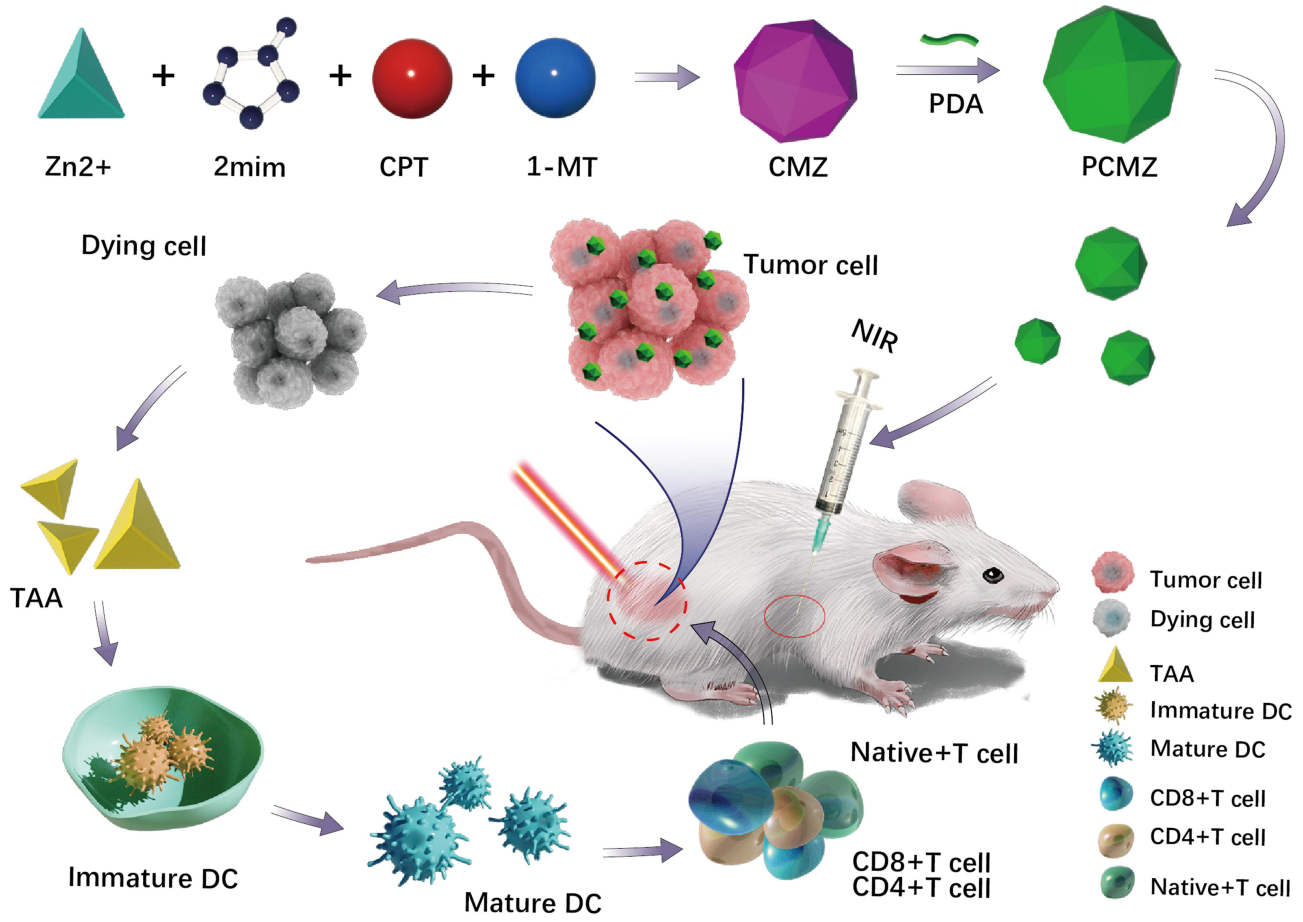

APC found so far, DCs can induce the production of specific cytotoxic T lymphocytes.[7] Tumors' occurrence and development are closely linked to DCs.[8]

Nevertheless, these mechanisms proved insufficient in controlling every aspect of the immune process required to trigger a robust cellular immune response against tumors. Numerous published works have attempted to combine various therapeutic substances within a framework in order to amplify the immune response against tumors. However, the designated function of each element in these compositions has not been optimized for an appropriate location, resulting in a significant decrease in their respective therapeutic effectiveness. The initiation of the body's antitumor immunity was anticipated through the release of damage-associated molecular patterns (DAMPs) and the production of tumor-associated antigens (TAAs) during the process of immunogenic cell death (ICD) in tumor cells.[9] DCs, the most proficient cells for presenting antigens, have the capability to internalize, process, and display antigens, thus initiating an immune response that leads to the subsequent generation of a powerful antitumor T cell response.[10,11] Hence, the crucial factor in triggering effective immunity was the strategic focus on nanoplatform design.

Photothermal therapy (PTT) is an innovative approach to combat tumors by efficiently eliminating cancer cells through the emission of thermal energy, along with the release of DAMPs and TAAs from the remnants of tumor cells.[12,13] In comparison to conventional subunit vaccines, the immunogenicity of cell residues after thermal ablation is enhanced. This enhanced immunogenicity fully triggers the immune response, leading to the development of antitumor antigen-specific immunity. Additionally, it can conquer the significant heterogeneity of tumors by releasing endogenous specific antigens.[14] In addition to insufficient antigen-specific activation, the clinical efficacy of immunotherapy is also

limited by the evolution of immune evasion caused by the tumor immunosuppressive microenvironment.[15,16] Indoleamine 2,3-dioxygenase (IDO), a modulatory enzyme mainly found in DCs, metabolizes tryptophan into kynurenine, resulting in the depletion of tryptophan and the elevation of immunosuppressive kynurenine.[17,18] To boost T-cell-mediated antitumor immunity and prevent immune evasion, 1-MT, widely recognized as the commonly employed IDO inhibitor.[19–21]

PDA is a favorable photothermal agent with good water solubility and biocompatibility. ZIF-8 NPs is a subtype of MOFs, a highly promising carrier, can use zinc ions and 2-methyl imidazole synthetic. With the advantages of good dispersion, large specific surface area, high porosity, and easy synthesis, ZIF-8 nanoparticles have been widely used in drug delivery, antibacterial therapy, and other fields.[22] Herein, we used ZIF-8 NPs with pH-sensitivity produced PDA/(1-MT+CPT) @ZIF-8 (PCMZ). The characterization of PCMZ NPs were measured by XRD, FTIR, TEM and DLS. The cytotoxicity and acute toxicity on mice were also measured. After that, anti-tumor activity was measured both in vivo and in vitro. Our formula, combination of PTT and immunotherapy, has the potential to eliminate not only the primary tumors but also hinder the growth of abscopal tumors. Additionally, it offers protection to the treated mice against the formation of rechallenged tumors.

Methods

Materials

Sinopharm Chemical Reagent Co., Ltd (Beijing, China) provided $Zn(NO_3)_2 \cdot 6H_2O$, 2-methylimidazole, and eosin. CPT, PDA, 1-MT, and kynurenine were obtained from Sigma-Aldrich located in Saint Louis, USA. Thermo Fisher Scientific (Waltham, USA) provided Dulbecco's modified eagle medium (DMEM), fetal bovine serum (FBS), and trypsin. The Annexin V-FITC kit, ROS assay kit, and DAPI were acquired from Beyotime Biotechnology Co., Ltd located in Shanghai, China. The Hematoxylin, HMGB1 kit, and ATP kit were acquired from Solarbio Biotechnology Co., Ltd located in Beijing, China. Abcam (Cambridge, MA, USA) was the source of the purchased antibodies for CAT, CD11c-FITC, CD80-APC, CD86-PE, CD8-PR, CD4-FITC, and CD3-APC proteins.

Vital River Laboratories (Beijing, China) supplied female BALB/c mice (6–8 weeks old), C57BL/6 mice (6–8 weeks old), and New Zealand rabbits (1-month old). The 4T1 and Vero cell lines were purchased Shanghai Gaining Biotechnology Co., Ltd (Shanghai, China) (Supplementary Materials).

Characterization of NPs

The morphology of NPs was examined using TEM (HT7700, Hitachi, Japan). The hydrodynamic particle size distribution and zeta potential of the NPs were determined using a Zetasizer (ZS90; Malvern Panalytical, Malvern, UK). The functional groups of NPs were characterized using a Fourier-transform infrared spectrometer (Excalibur HE 3100, Varian, USA). The crystal structure of the prepared nanoparticles was detected by X-ray diffraction (XRD). Cu Kα rays were used with a detection range of 5–50°.

Cell Culture

The culture medium for cells consisted of DMEM, 10% FBS, and antibiotics (100 U/mL penicillin and 100 μg/mL streptomycin). Cells were cultured at 37 °C using an incubator containing 5% CO_2. Prior to utilizing cells, they were collected through trypsinization and subsequently reconstituted in a new solution.

In vitro Drug Release

The flask was filled with 10 mg of PCMZ NPs suspended in PBS buffer (pH 7.4, 6.5, and 5.6) supplemented with 5% v/v DMSO. Samples were collected by centrifuging at regular intervals and collecting the resulting supernatants. The absorbance of supernatants at 366 nm and 287 nm (Different concentrations of CPT solution and 1-MT solution (methanol as solvent) were precisely prepared, and their absorption profiles at 200–800 nm were measured. The standard curves of the two drugs were plotted.) was measured to estimate the release of CPT and 1-MT, respectively.

Cellular Uptake and Location

The 24-well plates were applied to culture 4T1 cells. Then, the FITC encapsulated PCMZ at various concentrations were introduced into the plates for 4 h incubation. Then, the cells were washed with PBS twice and were fixed by 1% glutaraldehyde and 10% formaldehyde for 0.5 h. Fluorescence imaging was performed with a fluorescence microscope to monitor the cellular uptake of the NPs. The cell membrane imaging was performed with the DID. Briefly, after the cell incubation with PCMZ NPs for indicated time (0.5 h, 1 h, 2 h, and 4 h), the cells were washed twice with PBS and treated with DID for 30 min for lysosome staining.

Photothermal Effects in vitro

To investigate the photothermal effects of PCMZ NPs in a laboratory setting, we exposed NPs with varying concentrations (0, 100, 200, 300, 400, 500 μg/mL) to 808 nm near-infrared light for a duration of 5 minutes at an intensity of 1W/cm^2. The solution's temperature was analyzed and thermal images were captured using a thermal imager during the irradiation process.

In vitro Antitumor Study

4T1 cells were spread on 6-well plates at the concentration of 106 cells/well for 24 h, after which the medium was discarded, the medium containing NPs was added for a certain period of time, and the medium containing NPs was discarded and replaced with fresh maintenance medium. The cells were irradiated with 808 nm laser light at a power of 1 W/cm^2 for 3 min. The laser-treated cells were stained using Annexin V-FITC/PI double staining apoptosis detection kit, and the nuclei were labeled with DAPI and photographed under an inverted fluorescence microscope. In addition, the treated cells were washed and digested and re-hung in the buffer according to the kit instructions. Annexin V-FITC and PI staining were performed, respectively. After incubation, the cells were analyzed by flow cytometry.

Immunogenic Cell Death (ICD)

In order to investigate the PTT-induced ICD of 4T1 cells, we analyzed the in vitro expression of CRT, HMGB1, and ATP. In order to examine the presence of CRT on the surface of cells, 4T1 cells were placed in six-well microplates at a density of 3×10^5 cells per well and left to grow overnight. The following day, ZIF-8, CMZ, and PCMZ were administered to the cells. After one hour, the medium was substituted with a new maintenance medium, subsequently accompanied by the application or omission of an extra laser exposure at 808 nm (1 W/cm^2, 3 min). After applying various treatments, the cells were rinsed with PBS and then subjected to staining with Hoechst 33342. Next, the cells were immobilized using a fixative solution for 10 minutes at ambient temperature in preparation for the following staining with anti-CRT antibody and secondary antibody labeled with Alexa Fluor 488. In the end, a microscope was utilized to observe and capture images. Furthermore, the levels of HMGB1 and ATP in the supernatant were assessed following the guidelines provided with the kit.

In vitro DC Stimulation Experiments

BMDCs were derived from the bone marrow of C57BL/6 mice using previously described techniques and subsequently stained with anti-CD11c-FITC antibodies. Cells expressing CD11c were incubated with PCMZ and 1-MT for a duration of 24 hours. The concentration of 1-MT remained constant in all formulations. Following the incubation period, the cells were gathered and subjected to staining using antibodies against CD80-APC and CD86-PE. Flow cytometry was used to analyze cells that had been stained.

Cultured CD11C-positive cells were spread in the lower part of transwell chamber, and 4T1 tumor cells were spread in the upper part of transwell chamber. Culture medium containing 1-MT and PCMZ NPs was added for 1 h and then replaced with fresh maintenance medium. 4T1 cells were stimulated for 3 min by laser irradiation with the excitation wavelength of 808 nm and the power of 1 W/cm^2. Following 24 hours of uninterrupted cultivation, the culture medium was discarded, and subsequently, the underlying DCs were collected and purified using PBS. Fluorescent antibodies labeled cells were added and analyzed by flow cytometry.

Detection of IDO Activity on a Cellular Level

A previously described method, with minor modifications, was used to detect the inhibitory effects of 1-MT on the IDO pathway.[23] 4T1 cells were incubated onto 96-well dishes for one night. The next day, the cells were placed in a new solution with a certain concentration of L-tryptophan, interferon-γ, and with varying amounts of 1-MT (2, 5, 10, 20μg/mL). After 72 hours, 140 μL of the medium's supernatants were collected and subsequently mixed with 15 μL of 30% trichloroacetic acid at a temperature of 50 °C for 30 minutes to precipitate proteins. Following that, centrifugal force was utilized to eliminate precipitation. A volume of 100 μL of the supernatant was moved to a separate 96-well plate and combined with a 100 μL solution of acetic acid containing p-dimethylaminobenzaldehyde. Using a microplate reader, the absorbance at 480 nm was determined, and after constructing a standard curve for kyn, the concentration was calculated.

Antitumor Capacity in vivo Study

In order to assess the effectiveness of mixture against tumors, we injected 4T1 cells into the armpit of the right forelimb of BALB/c mice, resulting in the development of tumor-bearing mice. The mice with the tumor volume about 50–100 mm^3 were divided into four groups in a random manner. Subsequently, they were administered various samples through intravenous injection, including (1) saline; (2) CPT; (3) CMZ; (4) PCMZ (CPT (1 mg/kg) and 1-MT (1 mg/kg)). Following the administration, the groups of mice with tumors were subjected to an extra laser exposure of 808 nm after 24 hours of injection (1 W/cm^2, 5 min). While being exposed to radiation, a thermal imager captured infrared thermal images of mice with tumors. Every other day, tumor volume and body weight of each mouse were measured to calculate tumor inhibition ratio. The formula for calculating tumor volume is L multiplied by the square of W divided by 2. L refers to the longest diameter of tumors and W refers to the shortest diameter of tumors. The tumor inhibition ratio can be calculated by subtracting Wt from Wc, dividing the result by Wc, and then multiplying by 100%. The tumor weights of mice in the control group and the tumor weights of mice in the treated group are represented by Wc and Wt, respectively. Mice were sacrificed after 21 days. For histopathological assessment, tumors and major organs were separated, preserved in 10% formalin solution, and did H&E staining.

Abscopal Antitumor Effects

Mice with tumors on both sides were created by injecting 4T1 cells under the skin of the right armpit and then injecting 4T1 cells under the skin of the left armpit after 3 days. When the volumes of primary tumors reached 100 mm^3, mice were randomly divided into five groups, and then every 3 days treated with mixtures: (1) saline; (2) 1-MT; (3) CMZ; (4) PCMZ (CPT (1 mg/kg) and 1-MT (1 mg/kg)). At 6 h post-injection, the primary tumors in all groups were exposed to additional laser irradiation. Every 2 days, the sizes of initial tumors and distant tumors, along with the weights, were documented. After a period of 21 days, the mice were euthanized. Flow cytometry was used to analyze the $CD3^+/CD8^+$ T cells, $CD3^+/CD4^+$ T cells, and Tregs after collecting and homogenizing the spleens into single-cell suspension and staining them with corresponding antibodies.

Statistical Analysis

Statistical analyses were performed using GraphPad Prism 8.0 software. Data were analyzed by the two-sided *t* test. The levels of statistical significance are denoted as $*P < 0.05$, $**P < 0.01$, $***P < 0.001$ and $****P < 0.0001$.

Results and Discussion

Characterization of PCMZ

Both CPT and 1-MT were loaded in ZIF-8 NPs by "one pot" method like previous work.[22] Figure S1 showed the coordination modification of PDA on the surface of (CPT + 1-MT) @ ZIF-8 NPs, resulting in the formation of PDA/(CPT + 1-MT) @ ZIF-8 nanoparticles. Figure 1A illustrates the measurement of zeta potential for ZIF-8, (CPT+1-MT) @ZIF-8, and PDA/(CPT+1-MT) @ZIF-8. The zeta potential of ZIF-8 was determined to be 21.9 ± 4.65 mV, while (CPT +1-MT) @ZIF-8 exhibited a zeta potential of 19.6 ± 6.61 mV. On the other hand, PDA/(CPT+1-MT) @ZIF-8 displayed a zeta potential of −23.4 ± 4.83 mV. Due to the existence of loading with drug, part of drug was adsorbed on the surface

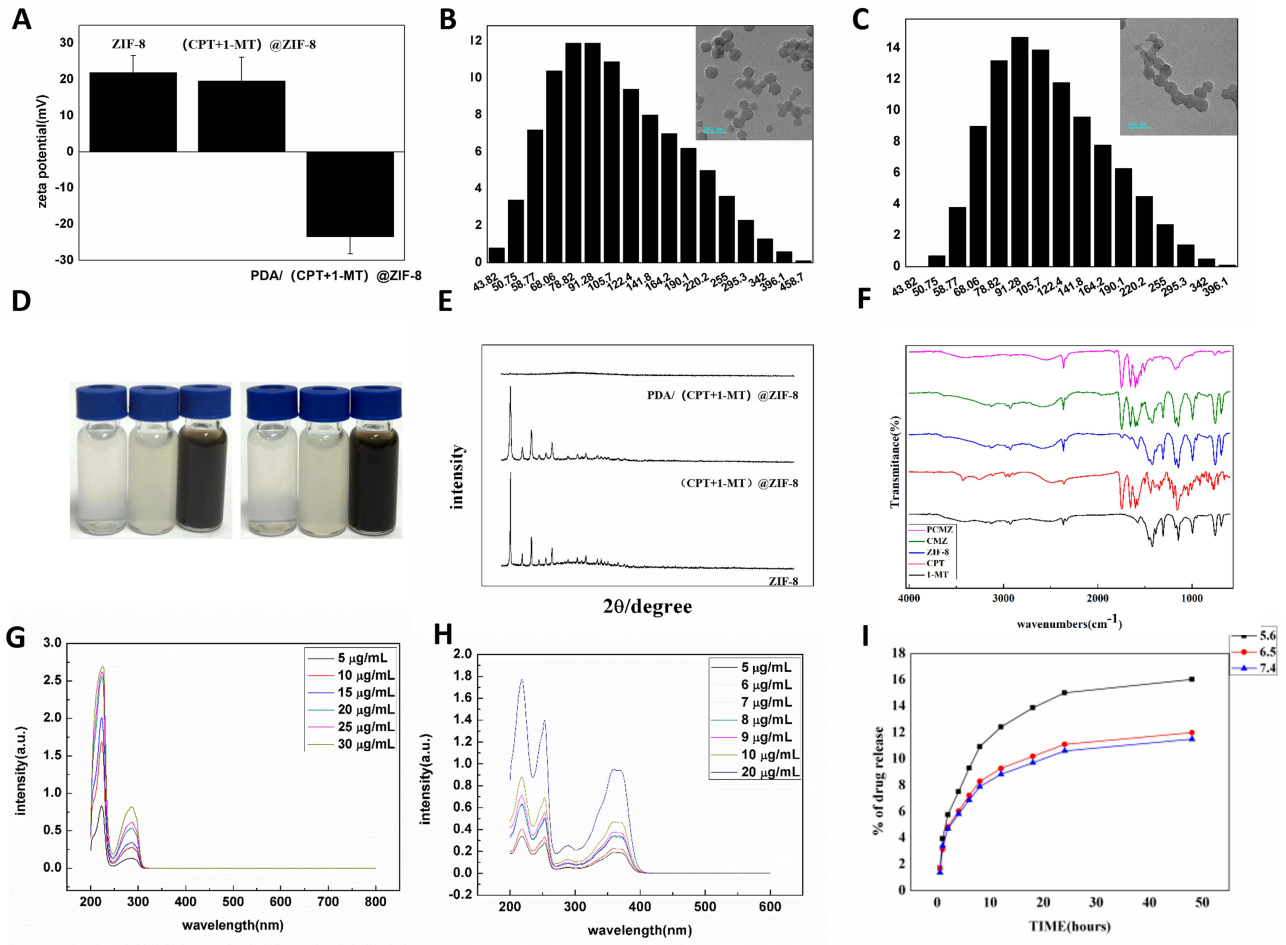

Figure 1 (**A**) The zeta potential of NPs, the TEM images and hydrodynamic size of (**B**) CMZ and (**C**) PCMZ, (**D**) The pictures of NPs on 0 day (left) and 7 days (right), ZIF-8, CMZ and PCMZ NPs respectively, (**E**) XRD and (**F**) FTIR spectra of NPs, (**G**) Ultraviolet-visible absorption spectra of 1-MT, (**H**) Ultraviolet-visible absorption spectra of CPT, (**I**) Drug release of PDA/(CPT+1-MT) @ZIF-8 NPs in different pH (5.6, 6.5 and 7.4).

through strong adsorption, and the potential after loading was lower than that of simple ZIF-8 NPs. The zeta potential of PDA modified NPs turned negative. The findings suggested that the negative charge exhibited increased stability and reduced biological toxicity following the successful modification of PDA and the NPs. The hydrated particle sizes of CMZ NPs and PCMZ NPs were 128.4 nm (polydispersity index = 0.126) and 132.6 nm (polydispersity index = 0.101), respectively (Figure 1B–C). The sizes did not vary significantly, and both CMZ NPs and PCMZ NPs exhibited the distinct hexahedral structure with well-defined edges and corners observed through TEM. This indicated that the morphology of ZIF-8 NPs remained unaffected by the modification of PDA, showing no significant impact. The CMZ NPs and PCMZ NPs acquired were effectively dispersed in water, remaining stable without any noticeable precipitation at 4 °C in darkness for a duration of 1 week (Figure 1D). Furthermore, the powder X-ray diffraction (XRD) technique was employed to assess the crystal structure of NPs. The peaks observed in Figure 1E for the synthesized ZIF-8 NPs and CMZ matched those of the standard ZIF-8, indicating that the synthesized particles possessed an identical crystal structure to the standard ZIF-8. While the PCMZ had no obvious peak due to the modification of PDA, it further confirmed the successful modification of PDA. The FTIR spectra of 1-MT, CPT, ZIF-8 NPs, CMZ and PCMZ are shown in Figure 1F; the PCMZ and CMZ had both absorption peaks of 1-MT, CPT and ZIF-8 NPS, which means the successful synthesized of PCMZ NPs as designed.

Figure 1G-H demonstrates that the CPT and 1-MT exhibited the highest absorption within the range of 200–400 nm. Consequently, a standard curve was constructed through linear regression analysis, utilizing drug concentration as the

x-axis and the absorbance at 280 nm for 1-MT and 360 nm for CPT as the y-axis. The standard of 1-MT and CPT was obtained (1-MT: y = 0.02634x - 0.00467, R2 = 0.99639, CPT: y = 0.05056x - 0.057, R2 = 0.9915). The measured quantity was the total volume of the solution obtained after the NPs process. The measurement of the UV absorbance of the liquid above was conducted. After replacing the data in the regression equation of the standard curve, the concentration of drugs in the supernatant was computed. The formula was used to calculate the entrapment efficiency (EE) and drug loading (DL). The EE of PCMZ NPs were 83.42% for 1-MT and 86.77% for CPT, respectively, which was similar to the drug encapsulation rate of previous studies.[24] The ZIF-8 NPs were regarded as the most promising drug carriers due to its excellent performance of pH-sensitivity. The drug release of different pH of PCMZ NPs were measured and 5.6, 6.5 and 7.4 of pH were elected. According to the illustration in Figure 1I, the initial 12 hours witnessed a swift drug release, which subsequently transitioned into a more consistent pattern. The drug release of 6.5 and 7.4 was basically the same, while a significant growth appeared of 5.6. This indicated a large release of drugs at tumor sites (acidic environment) and small release of drug at normal sites (neutral environment).

The Toxicity of PCMZ

The cell viability results were shown in Figure S2A. From the concentration of 0–200 μg/mL, only very low concentration (1.5625 μg/mL), the cell viabilities of ZIF-8, CMZ were up to 80%. However, after modification of PDA, even at the concentration of 200 μg/mL, the NPs also showed excellent cytocompatibility. The findings suggest that PCMZ NPs exhibit favorable biocompatibility when used as materials for drug delivery. The ROS produced by cells was further detected. DCFH was used to be a marker of ROS. In Figure S2B, blue fluorescence represents living cells, green fluorescence represents the production of ROS. There was no green fluorescence signal of the control group and PDA/(1-MT+CPT) @ZIF-8 group, while there was different strength of green fluorescent signal of the two groups treated with irradiation. This indicated that PDA/(1-MT+CPT) @ZIF-8 alone could not induce ROS production. As shown in Figure S2C, Triton-X 100 was set as positive group and normal saline was set as negative group, and the hemolysis of ZIF-8, CMZ and PCMZ was measured. At the concentration of 200 μg/mL and below, all NPs showed no hemolysis (<5%), and when 250 μg/mL, PCMZ still showed no hemolysis, but the hemolysis rates of ZIF-8 and CMZ were more than 5%. Overall, PCMZ has good hemolytic safety to meet the requirements of hemolysis testing.

In a previous report, the toxicity of ZIF-8 NPs was investigated, and the target organs of toxicity were liver and lung.[25] Therefore, the toxicity of PCMZ was further studied in vivo. All mice in the experimental group showed no abnormal performance. Pathological sections of main organs showed no obvious lesions (Figure S2D), which showed the modification of PDA reduced ZIF-8 toxicity.

The Photothermal Performance of PCMZ in vitro

The photo-sensitivity of the PCMZ NPs was confirmed by irradiated with 808 nm laser with an intensity of 1 W/cm2. The correlation of temperature rise with concentration and time was verified. Figure 2A–B displays the temperature trend of PCMZ NPs. The control group consisted of pure water (ΔT = 1.1°C). Under irradiation, at a concentration of 500 μg/mL, the temperature rose to 62.3°C within 15 minutes (ΔT = 37.3°C). At the beginning of irradiation, the temperature raised rapidly and tended to be stable at about 8 min. Once removed the irradiation, the temperature decreased rapidly, the irradiation continued to provide, and the temperature repeated to high (Figure 2C). The fluorescence spectrum of ZIF-8, CMZ, and PCMZ is displayed in Figure 2D. Among them, only PCMZ NPs exhibited a significant absorption within the 600–850 nm range, which falls within the "phototherapy window". These findings suggest that PCMZ NPs possessed excellent photothermal capabilities, primarily attributed to PDA.

Cellular Uptake Behavior and the Effects on Apoptosis of 4T1 Cells

The PCMZ-FITC was synthesized to measure the cellular uptake. DID and DAPI staining were used to label the cells, and the green fluorescent signal of FITC was used to be a marker of NPs. The green fluorescence signal appeared at 30 min and reached the maximum at 1h, gradually attenuated in the following 4h (Figure 3). To identify the deceased and viable cells, the Annexin-V-FITC/PI dual-staining method was employed. As shown in Figure 4A, Q4 means the living cells, Q3 means the early apoptotic cells, Q2 means the advanced apoptotic cells, and Q1 means the necrotic cells. The

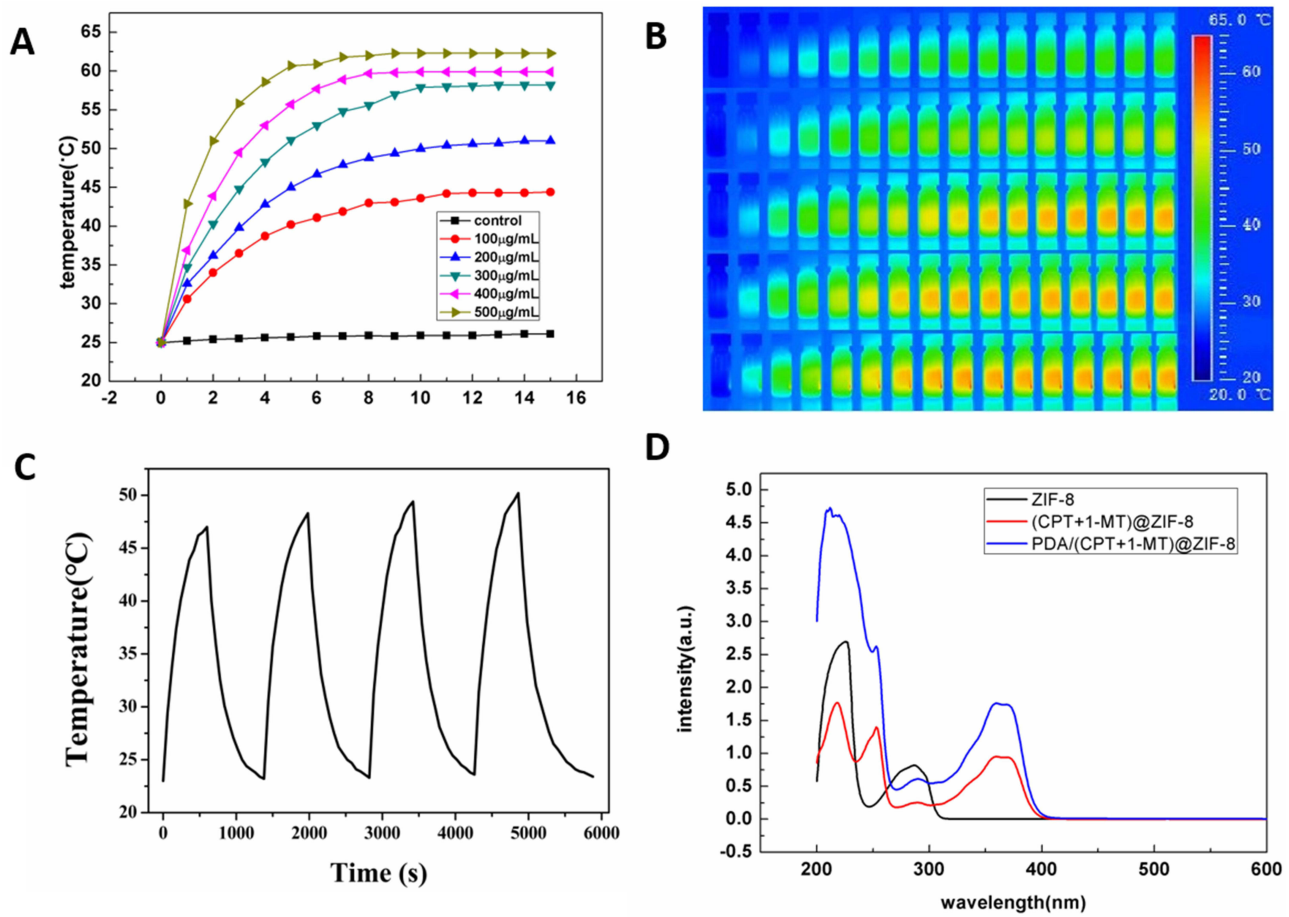

Figure 2 (**A**) The optical photographs and (**B**) thermal image of PDA/(CPT+1-MT) @ZIF-8 NPs at different concentrations in water after 808nm laser irradiation, (**C**) The temperature variations of PDA/(CPT+1-MT) @ZIF-8 NPs at 200 μg/mL under 808 nm laser irradiation for 4 cycles, (**D**) Ultraviolet-visible absorption spectra of ZIF-8, (CPT +1-MT) @ZIF-8 NPs and PDA/(CPT+1-MT) @ZIF-8 NPs.

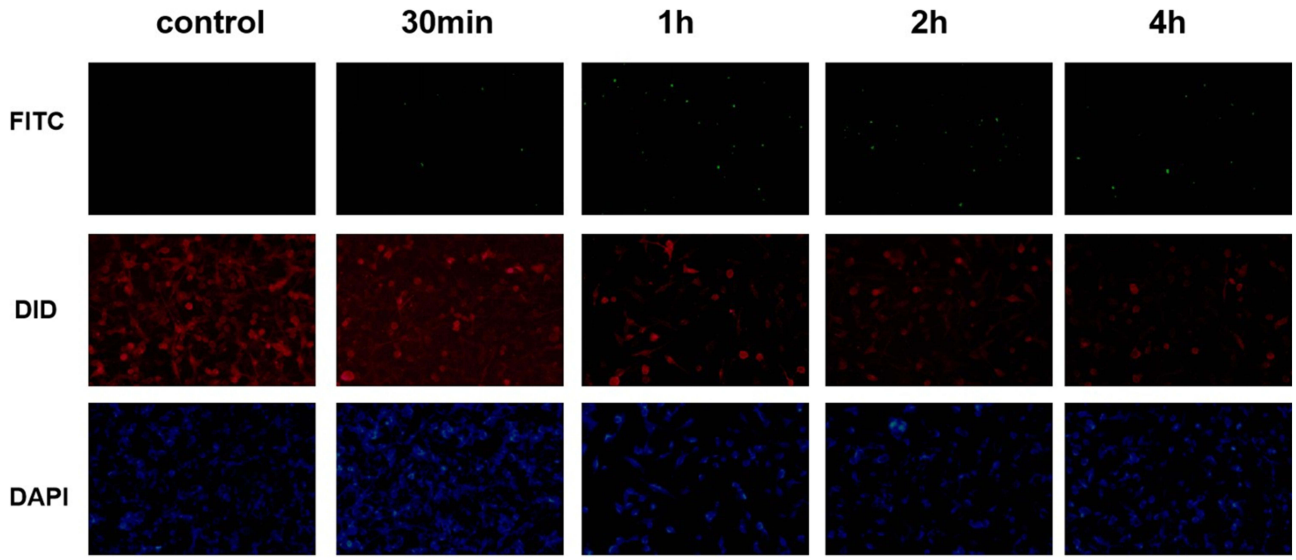

Figure 3 The cellular uptake capacity of PDA/(CPT+1-MT) @ZIF-8.

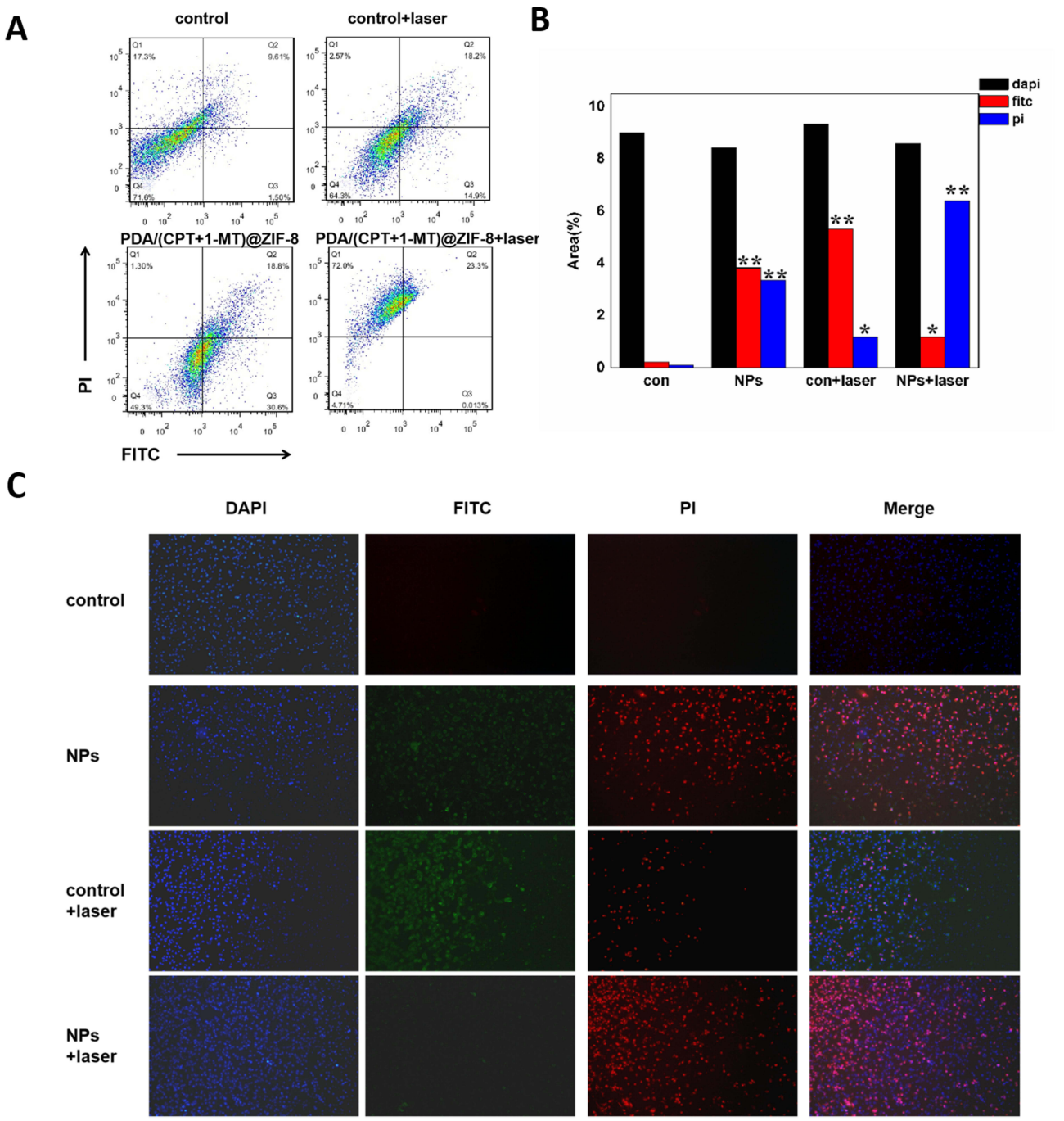

Figure 4 (**A**) Flow cytometry analysis about the apoptosis and necrosis of 4T1 cells of different treatment, (**B**) Quantitative of fluorescent images of 4T1 cells treated with PCMZ NPs under 808 nm laser irradiation, *, $P < 0.05$, **, $P < 0.01$, (**C**) Fluorescent images of 4T1 cells treated with PCMZ NPs under 808 nm laser irradiation.

application of PCMZ resulted in an increase in apoptotic cells compared to the control group, as did the control group that underwent irradiation treatment. Meanwhile, the cell treated with both PCMZ and irradiation showed a large number of necrotic cells. To identify the deceased and viable cells, the Annexin-V-FITC/PI dual-staining technique was employed. Figure 4B–C displays the findings. Blue staining indicated living cells, green staining indicated early apoptotic cells, both green and red staining indicated advanced apoptotic cells, and red staining indicated necrotic cells. After laser irradiation alone, a small amount of apoptosis was observed in 4T1 cells, and large amounts of apoptotic cells in group treated with PCMZ. Moreover, when laser irradiation was added, the necrosis rate of 4T1 cells increased

remarkably. Those results showed PCMZ nanomaterials under 808 nm laser irradiation had strong ability to kill tumor cells. Photothermal therapy is a minimally invasive therapy for tumor developed in recent years, which mainly converts light energy into heat energy through photothermal conversion agents, so as to achieve thermal ablation of tumor and finally achieve the purpose of tumor treatment.[26]

The Effect of PCMZ NPs on IDO Activity and DC Stimulation in vitro

Evidence indicated that immature DCs can undergo maturation when exposed to antigens and adjuvants, resulting in the presentation of antigens on their surface, subsequent activation of T cells, and the initiation of an immune response.[27,28] The immunostimulatory effects of PCMZ were examined by flow cytometry (Figure 5A) to analyze the expression of CD80/CD86 on BMDCs. The discovery revealed that one metric ton could greatly increase the expression of CD80/CD86. Significantly, PCMZ has the potential to induce further maturation of BMDCs. The flow cytometry results of BMDCs maturation stimulated by 4T1 cells in different treatments are shown in Figure 5B. The 1-MT group showed a significant increase compared to the control group. And $CD80^+/CD86^+$ DCs in PCMZ nanoparticle group and PMCZ nanoparticle + laser group were significantly further increased, which were 25.15%±1.69% and 35.78%±1.82%, respectively. The findings from DC stimulation experiments indicated that the remnants of tumor cells, which were a result of PTT and PCMZ NPs, collaborated to augment the DCs' activation and maturation, thereby bolstering the robust immune response. Currently, dendritic cells are the most potent cells for presenting antigens and they have a crucial function in the immune response against tumors.[29] Mature DCs highly expressed MHC II class molecules, CD40, CD80, CD86 and other adhesion molecules, so mature DCs had strong antigen presentation ability. Immature DCs cannot activate T cells and can only activate T cells when differentiated into mature DCs. Some scholars believe that DC is the only antigen-presenting cell that can effectively activate initial cytotoxic T cell nucleus initial helper T cells.[30,31] The discovery revealed that one metric ton could greatly increase the expression of CD80 and CD86. Significantly, the ZIF-8 encapsulation and PDA modification could additionally induce maturation of BMDCs.

By examining the IDO marker expression, the immunostimulatory impacts of PCMZ were investigated. IDO catalyzed tryptophan to produce kynurenine, which had the capability to inhibit the immune response against tumors. Consequently, the inhibitory capacity of the IDO pathway was evaluated in BMDCs that exhibited a high expression of IDO. As depicted in Figure 6A, the suppression of kyn was intensified as the levels of 1-MT rose within the examined range of concentrations. Presently, the concepts of "tryptophan deprivation" and "toxic effects of metabolites" are widely employed to elucidate the role of IDO in evading the immune system.[32] In tumor cells, the high expression of IDO leads to the depletion of tryptophan in the tumor microenvironment, which inhibits T cells in G1 phase, thus inducing the

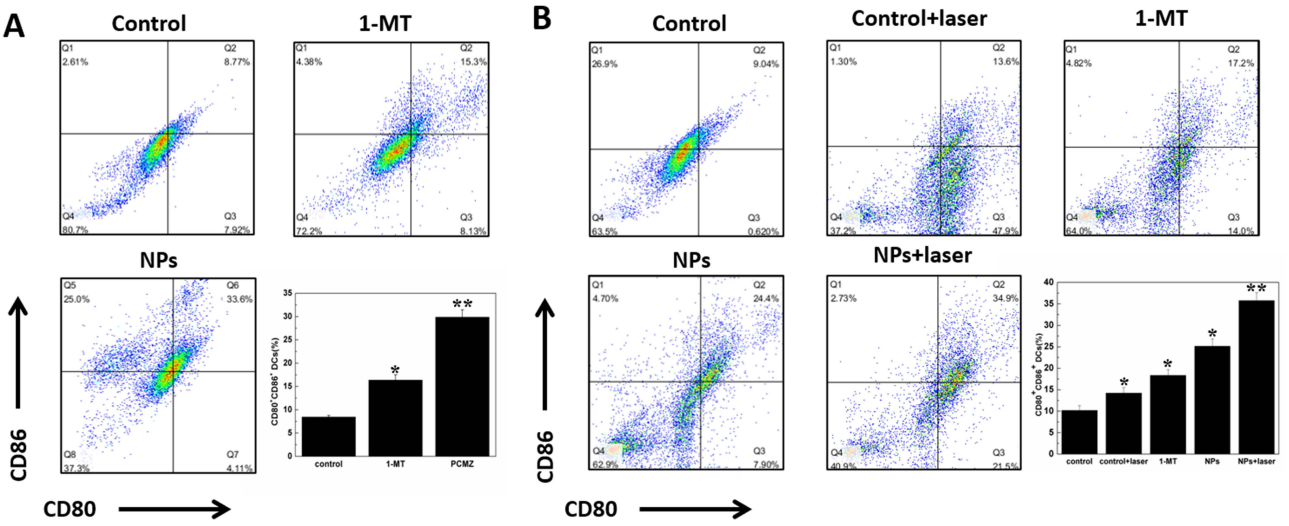

Figure 5 (**A**) Flow cytometric results of mature BMDCs simulated by 1-MT and PCMZ NPs, (**B**) Flow cytometric results of mature BMDCs simulated by 4T1 cells treated with 1-MT and PCMZ NPs.

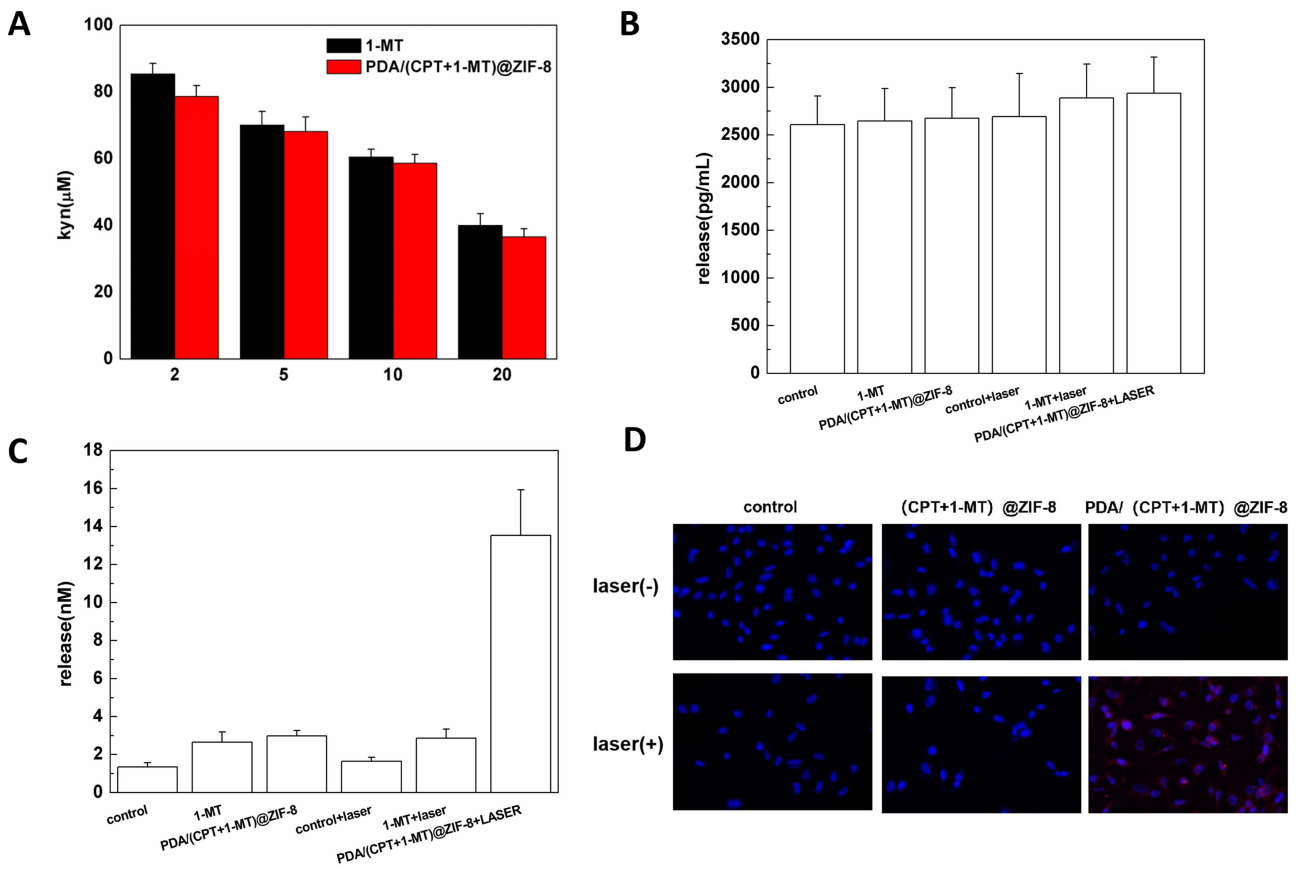

Figure 6 (**A**) The concentration of kyn on 4T1 cells treated with 1-MT and PCMZ NPs, level of (**B**) HMGB and (**C**) ATP of supernatant 4T1 cells treated with NPs under 808 nm laser irradiation, (**D**) Immunofluorescence pictures of CRT on 4T1 cells treated with mixtures.

apoptosis of T cells and further generating immune escape. Compared with 1-MT, the kyn content in 4T1 cells treated with PCMZ NPs at the same concentration was lower. The effectiveness of PCMZ NPs in inhibiting the IDO pathway was demonstrated, highlighting the remarkable inhibitory capability of PCMZ on the IDO pathway. The trend was generally in line with previous reports.[15,33]

The initiation of the immune response against tumors was associated with the manner in which cancer cells underwent cell death.[34] The activation of immune response was anticipated when ICD, triggered by intense cellular stress responses like PTT, caused the release of DAMPs.[35] Li et al designed to load IR-7 into liposomes and graft immune preparation CpG on the surface of liposomes. After intravenous injection of the liposomes, the liposomes were enriched at the tumor site. At the same time, it promotes the release of DAMPs from tumor cells, which in combination with CpG, promotes antigen presentation and activates the immune system of the body to achieve effective inhibition of metastatic tumor cells.[36] Hence, the investigation of high mobility group box 1 (HMGB1) was conducted to assess the presence of ICD indicators. The presentation of calreticulin (CRT) on the surface of cells, a protein associated with ICD, may lead to the generation of a signal indicating "consume me", which can activate the immune response against tumors. According to reports, HMGB1 has been identified as a signal of danger that promotes the phagocytosis of dying tumor cells by DCs.[37]

As shown in Figure 6B-C, the levels of HMGB1 and ATP were measured, the cells treated with PCMZ and irradiation show a raise on both HMGB1 and ATP, which means the treatment induced the ICD of cells. The immunofluorescence staining of CRT shown in Figure 6D also proved it. The study utilized immunofluorescence staining to identify the CRT signal. The results revealed that solely the PCMZ + laser group exhibited the CRT signal, suggesting that only the successful photothermal effect facilitated by PCMZ particles could trigger immunogenic death of 4T1 cells. The

increased HMGB1 and ATP in the cell supernatant of PCMZ + laser group further proved that the effective photothermal effect mediated by PCMZ NPs could induce immunogenic death of 4T1 cells.

In vivo Anti-Tumor Study

In the previously mentioned in vitro tests, the tumor cell remnants generated by the PCMZ-facilitated PTT could significantly enhance the maturation of DCs in the presence of 1-MT adjuvants within PCMZ. Afterwards, fully developed DCs were capable of effectively stimulating T cell growth, and the presence of 1-MT in PCMZ could disrupt the suppressive kynurenine pathway, thereby enhancing the robust immune response in a synergistic manner. The combination of potent PTT and robust immune response showed great potential for the revolutionary anti-cancer treatment. We conducted a study to examine the effectiveness of tumor-bearing mice models in inhibiting tumor growth in living organisms (Figure 7A). After PCMZ administration, the tumor regions of mice were exposed to an 808 nm laser for a duration of 8 minutes. The curves depicting the rise in temperature and the infrared thermal images (Figure 7B-C) demonstrated that the tumor temperature in mice treated with these compounds could elevate by around 34.1 °C and reach 61.8 °C (ΔT = 27.7°C). This temperature increase was sufficient to eradicate tumor cells and hinder the malignant growth of tumors. The enhanced survival rate of mice with tumors (Figure 7D) can be attributed to the inhibited advancement of the tumor and minimal adverse reactions caused by our formulations. As shown in Figure 7E–G, the

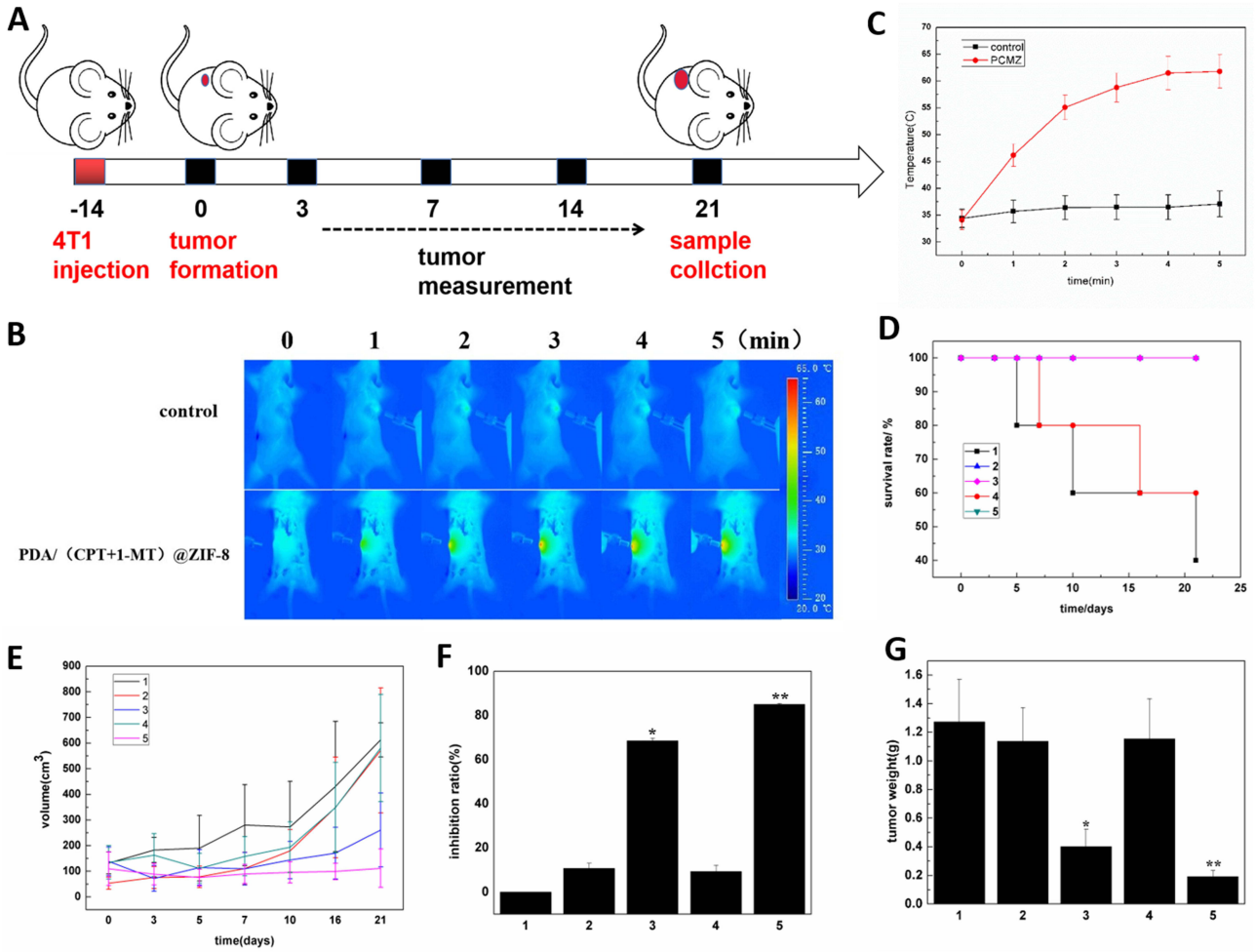

Figure 7 (**A**) Schematic illustration of therapy in an tumor-bearing model, (**B**) Thermal imaging of tumor in tumor-bearing mice treated with PCMZ under 808 nm laser irradiation, (**C**) Temperature curve of PCMZ in tumor-bearing mice under 808 nm laser irradiation, (**D**) The survival rate, (**E**) The volumes of tumor, (**F**) The inhibition ratio, (**G**) The weight of tumor of mice after different treatments (1: Control group, 2: CPT groups, 3: PCMZ groups, 4: Control + laser groups, 5: PCMZ + laser groups). *, $P < 0.05$, **, $P < 0.01$.

tumor volumes of mice treated with PCMZ and irradiation were 111.65 ± 74.98 cm^3, while the control groups were 612.34 ± 166.34 cm^3. All data proved the treatment were good behaved in tumor inhibition effect in vivo.

Furthermore, main organs and tumors collected were subjected to histopathological examination using hematoxylin and eosin (H&E) staining. The organs isolated from the mice in the treatment groups showed no noticeable morphological changes compared to those in the control group (Figure 8), indicating a low level of toxicity on normal tissues. Interestingly, the tumors treated with PCMZ exhibited more pronounced cell damage (as shown by the arrow), particularly severe in nature. The results strongly indicated that our formula has an antitumor synergy under the combined action of PTT and immunotherapy with low toxicity and side effects, which is expected to be further applied in clinical antitumor therapy.

The Effects of Abscopal Antitumor Therapy

Given the above experimental results, bilateral tumor models were established in mice by inoculating 4T1 cells in both the left and right axilla. The left tumor served as the primary tumor, while the right tumor acted as the metastatic tumor (Figure 9A). The inhibitory effect of PCMZ + laser on the primary and metastatic tumor of mice was evaluated. The examination of the tumor sizes, tumor masses, and tumor suppression rates (Figure 9B–G) revealed swift tumor expansion in the control group treated with normal saline, whereas tumors displayed somewhat slowed growth rate following the administration of PCMZ group due to the systemic immunotherapy. For the primary tumor, the tumor inhibitory rate of PCMZ NPs was 61.42%±3.11%, and that of PCMZ + laser group was 82.61%±5.65%. The inhibitory

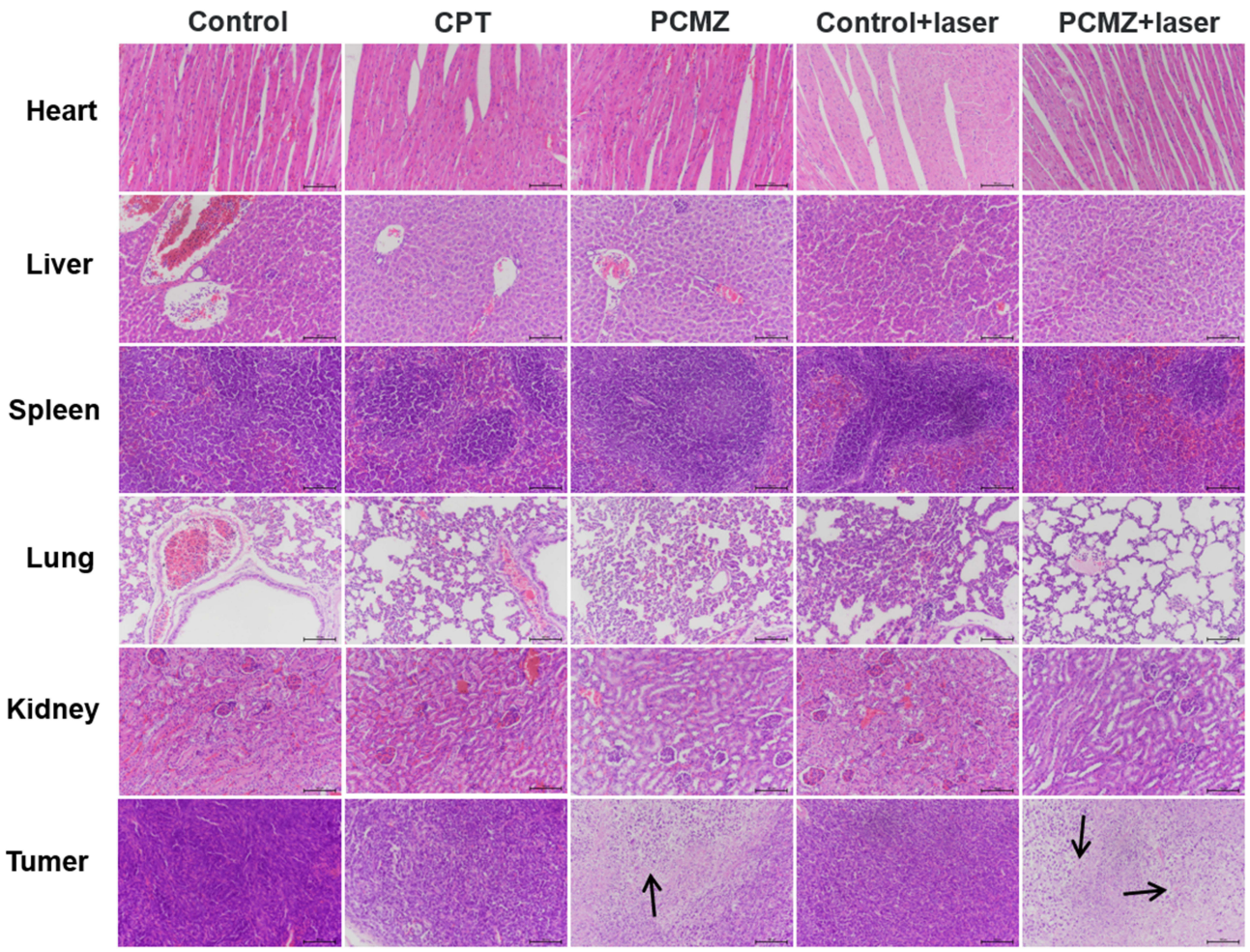

Figure 8 H&E staining results of major organs (heart, liver, spleen, lung and kidney) and tumors for all tested groups in tumor-bearing mice (more pronounced cell damage as shown by the arrow).

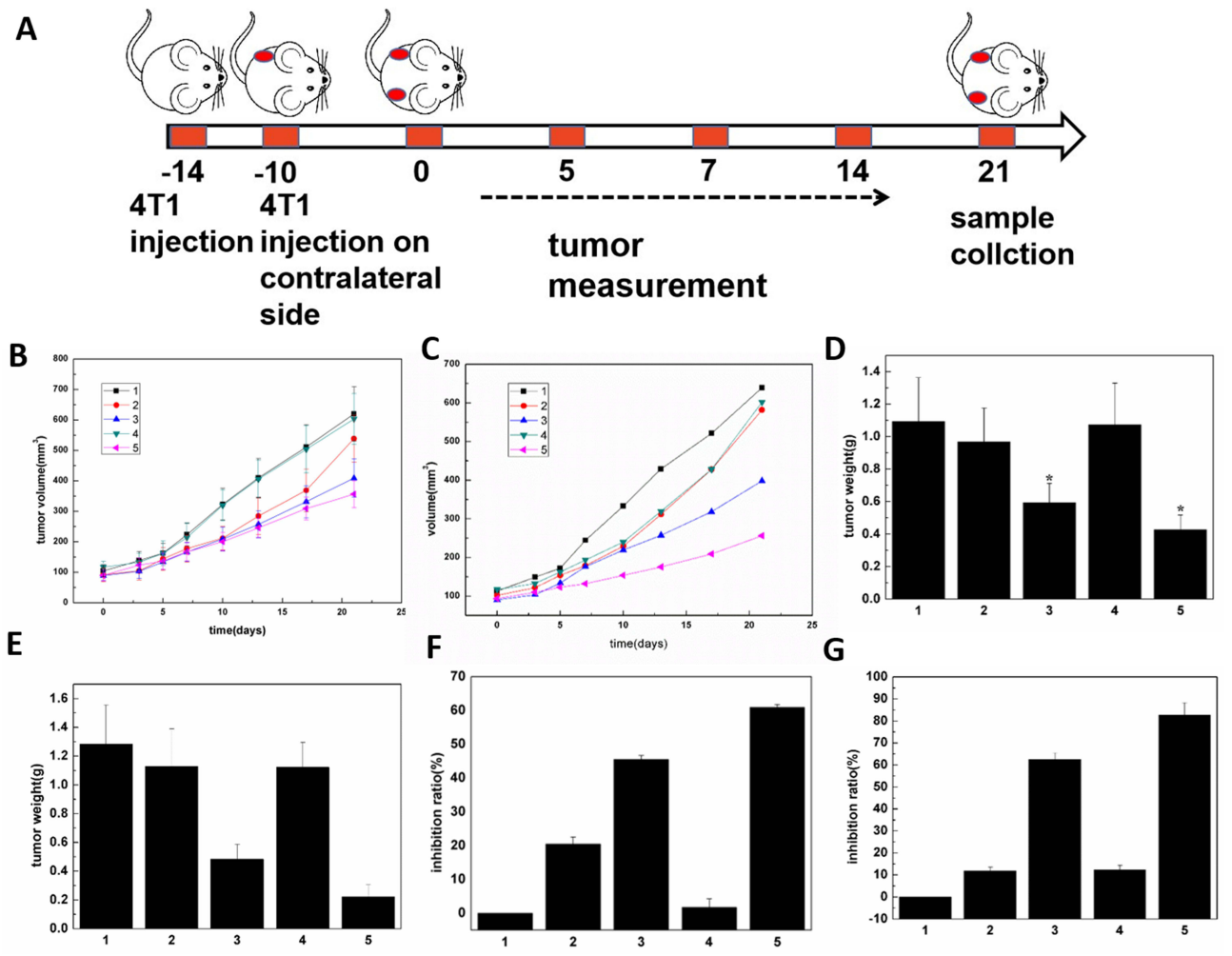

Figure 9 (**A**) Schematic illustration of therapy in a bilateral tumor-bearing mice model, The volumes of (**B**) primary tumor and (**C**) metastatic tumor, the inhibition ratio of (**D**) primary tumor and (**E**) metastatic tumor, The weight of (**F**) primary tumor and (**G**) metastatic tumor in mice after different treatments (1: Control group, 2: CPT groups, 3: PCMZ groups, 4: Control + laser groups, 5: PCMZ + laser groups).

effect of PCMZ NPs on the primary tumor was mainly due to the photothermal effect of CPT and PDA. When combined with tumor volume, tumor weight, and tumor inhibitory rate, the photothermal group did not show any impact on metastatic tumors. On the other hand, the 1-MT group exhibited a slight inhibition in tumor growth, while the PCMZ nanoparticle group effectively suppressed the growth of metastatic tumors. The PCMZ + laser group demonstrated the most potent inhibitory effect on metastatic tumors. The results showed that laser radiation by itself did not have any inhibitory impact on metastatic tumors. However, the PCMZ NPs exhibited a suppressive effect on metastatic tumors, primarily due to the presence of 1-MT. Additionally, the application of photothermal therapy increased the inhibitory effect of PCMZ NPs on tumors. As shown in Figure S3, no significant pathological changes were observed in other major organs in each group, but extensive necrosis was observed in the primary and metastatic tumor cells in PCMZ and PCMZ + laser group (as pointed by the arrow).

In order to elucidate the process of enhanced antitumor cellular immunity induced by our preparations, we gathered the untreated distant tumors and analyzed the T lymphocytes in the spleen using flow cytometry. The proportions of $CD3^+/CD4^+$ T cells and $CD3^+/CD8^+$ T cells significantly enhanced after the 1-MT treatment. Furthermore, the proportions of $CD4^+$ T lymphocytes and $CD8^+$ T lymphocytes also demonstrated a significant rise in the spleen of mice subjected to PCMZ treatment and a combination of PCMZ treatment with irradiation (Figure 10A–B). The strong cellular immunity, primarily caused by the inclination of T lymphocytes, effectively inhibited abscopal tumors. Recent findings

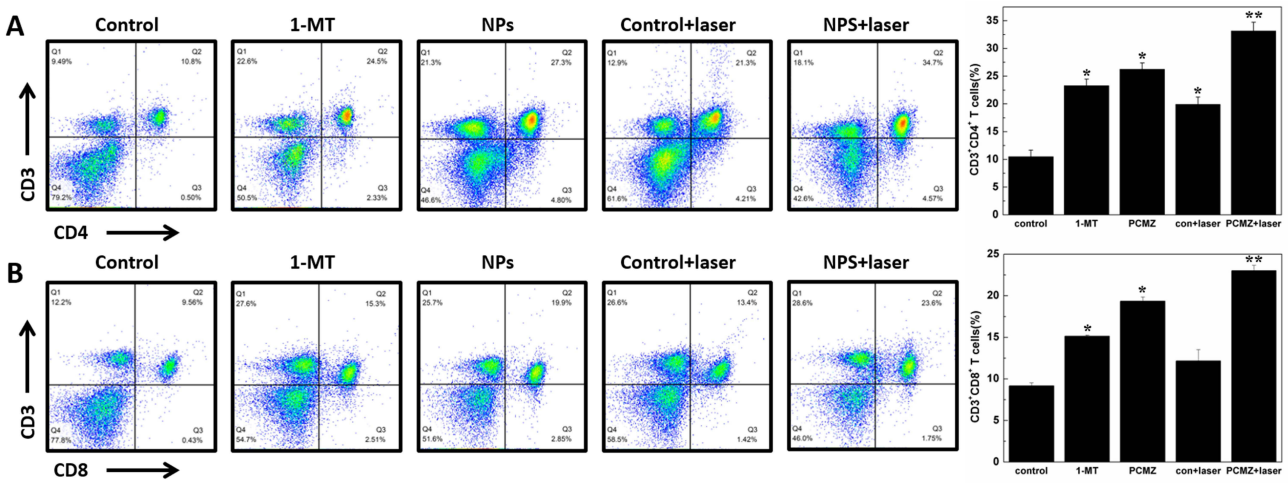

Figure 10 Flow cytometric results of (**A**) $CD3^+/CD4^+$T cells and (**B**) $CD3^+/CD8^+$T cells in spleen from bilateral tumor-bearing mice model. *$P < 0.05$, **$P < 0.01$.

have elucidated that $CD8^+$ T cells possess the ability to directly target cancerous cells by releasing cytotoxins.[38] Conversely, $CD4^+$ T cells assumed crucial functions in governing an adaptive immune response.[39]

To summarize, PCMZ NPs have the ability to trigger immunogenic cell death in tumor cells, promote the maturation of DCs, drive the differentiation of T cells into both helper T cells and cytotoxic T cells, and suppress the IDO pathway to overcome the inhibitory effect of IDO on T cells, ultimately leading to the eradication of tumor cells.

Conclusion

Herein, a novel immunotherapeutic nanoplatform was developed and built, in which camptothecin and 1-MT were successfully loaded into ZIF-8 NPs by one-pot method. In this study, chemotherapy, photothermal and immunotherapy were integrated into a nano-material, and the construction of a multifunctional carrier was realized. The combination of chemotherapy-induced apoptosis, PDA-mediated photothermal and nano-particle-mediated T cell activation provides a novel anti-tumor mechanism. The findings indicated the PCMZ effectively enhanced the development of DCs in vitro, which collaborated with 1-MT to enhance T cell growth. The findings in vivo showed the PCMZ NPs induced a remarkable systemic immune reaction and generated effects of immunological memory to combat metastatic and rechallenged tumors. Consequently, our approach focused on the collaboration of different therapeutic agents in terms of space and time, shows immense potential in overcoming challenges faced by antitumor immunotherapy. It provides a powerful framework for tumor immunotherapy. Although this study has proved that, under 808 nm laser irradiation PCMZ NPs can induce apoptosis of tumor, but the metabolic distribution of CPT in animals is still unclear, nanoparticles in the apoptosis of CPT in what is the function of the unknown need to be further in-depth study.

Ethics Approval and Consent to Participate

Animal experimentation was conducted according to the Regulations of Experimental Animals of Beijing Authority and approved by the Animal Ethics Committee of the China Agricultural University (cau20210619-3).

Funding

This study was funded by National Natural Science Foundation of China (Project No. 31772702), and Beijing Natural Science Foundation (Project No. 6202017).

Disclosure

The authors report no conflicts of interest in this work.

References

1. Irvine DJ, Hanson MC, Rakhra K, Tokatlian T. Synthetic nanoparticles for vaccines and immunotherapy. *Chem Rev*. 2015;115(19):11109–11146. doi:10.1021/acs.chemrev.5b00109
2. Xu J, Xu L, Wang C, et al. Near-infrared-triggered photodynamic therapy with multitasking upconversion nanoparticles in combination with checkpoint blockade for immunotherapy of colorectal cancer. *ACS nano*. 2017;11(5):4463–4474. doi:10.1021/acsnano.7b00715
3. Mellman I, Coukos G, Dranoff G. Cancer immunotherapy comes of age. *Nature*. 2011;480(7378):480–489. doi:10.1038/nature10673
4. Ng CW, Li J, Pu K. Recent progresses in phototherapy-synergized cancer immunotherapy. *Adv Funct Mater*. 2018;28(46). doi:10.1002/adfm.201804688
5. Yang X, Lian K, Meng T, et al. Immune adjuvant targeting micelles allow efficient dendritic cell migration to lymph nodes for enhanced cellular immunity. *ACS Appl Mater Interfaces*. 2018;10(39):33532–33544. doi:10.1021/acsami.8b10081
6. Chen Q, Hu Q, Dukhovlinova E, et al. Photothermal therapy promotes tumor infiltration and antitumor activity of car t cells. *Ad. Mater*. 2019;31(23):e1900192. doi:10.1002/adma.201900192
7. Wong JL, Mailliard RB, Moschos SJ, et al. Helper activity of natural killer cells during the dendritic cell-mediated induction of melanoma-specific cytotoxic T cells. *J Immunother*. 2011;34(3):270–278. doi:10.1097/CJI.0b013e31820b370b
8. Yang G, Xu L, Chao Y, et al. Hollow MnO(2) as a tumor-microenvironment-responsive biodegradable nano-platform for combination therapy favoring antitumor immune responses. *Nat Commun*. 2017;8(1):902. doi:10.1038/s41467-017-01050-0
9. Duan X, Chan C, Lin W. Nanoparticle-mediated immunogenic cell death enables and potentiates cancer immunotherapy. *Angew Chem*. 2019;58(3):670–680. doi:10.1002/anie.201804882
10. Hamdy S, Haddadi A, Hung RW, Lavasanifar A. Targeting dendritic cells with nano-particulate PLGA cancer vaccine formulations. *Adv Drug Delivery Rev*. 2011;63(10–11):943–955. doi:10.1016/j.addr.2011.05.021
11. Dewitte H, Verbeke R, Breckpot K, De Smedt SC, Lentacker I. Nanoparticle design to induce tumor immunity and challenge the suppressive tumor microenvironment. *Nano Today*. 2014;9(6):743–758. doi:10.1016/j.nantod.2014.10.001
12. Zhou F, Yang J, Zhang Y, et al. Local phototherapy synergizes with immunoadjuvant for treatment of pancreatic cancer through induced immunogenic tumor vaccine. *Clin Cancer Res*. 2018;24(21):5335–5346. doi:10.1158/1078-0432.Ccr-18-1126
13. Wang T, Zhang H, Han Y, et al. Light-enhanced o(2)-evolving nanoparticles boost photodynamic therapy to elicit antitumor immunity. *ACS Appl Mater Interfaces*. 2019;11(18):16367–16379. doi:10.1021/acsami.9b03541
14. Chen Q, Xu L, Liang C, Wang C, Peng R, Liu Z. Photothermal therapy with immune-adjuvant nanoparticles together with checkpoint blockade for effective cancer immunotherapy. *Nat Commun*. 2016;7:13193. doi:10.1038/ncomms13193
15. Ye Y, Wang J, Hu Q, et al. Synergistic transcutaneous immunotherapy enhances antitumor immune responses through delivery of checkpoint inhibitors. *ACS nano*. 2016;10(9):8956–8963. doi:10.1021/acsnano.6b04989
16. Moon YW, Hajjar J, Hwu P, Naing A. Targeting the indoleamine 2,3-dioxygenase pathway in cancer. *J Immunotherap Cancer*. 2015;3:51. doi:10.1186/s40425-015-0094-9
17. Araújo EF, Loures FV, Bazan SB, et al. Indoleamine 2,3-dioxygenase controls fungal loads and immunity in Paracoccidioidomicosis but is more important to susceptible than resistant hosts. *PLoS Negl Trop Dis*. 2014;8(11):e3330. doi:10.1371/journal.pntd.0003330
18. Lu K, He C, Guo N, et al. Chlorin-based nanoscale metal-organic framework systemically rejects colorectal cancers via synergistic photodynamic therapy and checkpoint blockade immunotherapy. *J Am Chem Soc*. 2016;138(38):12502–12510. doi:10.1021/jacs.6b06663
19. Calleja P, Irache JM, Zandueta C, Martínez-Oharriz C, Espuelas S. A combination of nanosystems for the delivery of cancer chemoimmunotherapeutic combinations: 1-Methyltryptophan nanocrystals and paclitaxel nanoparticles. *Pharmacol Res*. 2017;126:77–83. doi:10.1016/j.phrs.2017.09.004
20. Soliman HH, Minton SE, Han HS, et al. A Phase I study of indoximod in patients with advanced malignancies. *Oncotarget*. 2016;7(16):22928–22938. doi:10.18632/oncotarget.8216
21. Moreno AC, Clara RO, Coimbra JB, et al. The expanding roles of 1-methyl-tryptophan (1-MT): in addition to inhibiting kynurenine production, 1-MT activates the synthesis of melatonin in skin cells. *FEBS J*. 2013;280(19):4782–4792. doi:10.1111/febs.12444
22. Zhang H, Jiang W, Liu R, et al. Rational design of metal organic framework nanocarrier-based codelivery system of doxorubicin hydrochloride/verapamil hydrochloride for overcoming multidrug resistance with efficient targeted cancer therapy. *ACS Appl Mater Interfaces*. 2017;9(23):19687–19697. doi:10.1021/acsami.7b05142
23. Wang N, Wang Z, Xu Z, Chen X, Zhu G. A cisplatin-loaded immunochemotherapeutic nanohybrid bearing immune checkpoint inhibitors for enhanced cervical cancer therapy. *Angew Chem Int Ed Engl*. 2018;57(13):3426–3430. doi:10.1002/anie.201800422
24. Dong K, Zhang Y, Zhang L, Wang Z, Ren J, Qu X. Facile preparation of metal-organic frameworks-based hydrophobic anticancer drug delivery nanoplatform for targeted and enhanced cancer treatment. *Talanta*. 2019;194:703–708. doi:10.1016/j.talanta.2018.10.101
25. Su L, Wu Q, Tan L, et al. High biocompatible zif-8 coated by zro(2) for chemo-microwave thermal tumor synergistic therapy. *ACS Appl Mater Interfaces*. 2019;11(11):10520–10531. doi:10.1021/acsami.8b22177
26. Sheng W, He S, Seare WJ, Almutairi A. Review of the progress toward achieving heat confinement-The holy grail of photothermal therapy. *J Biomed Opt*. 2017;22(8):80901. doi:10.1117/1.Jbo.22.8.080901
27. Liu YJ. Dendritic cell subsets and lineages, and their functions in innate and adaptive immunity. *Cell*. 2001;106(3):259–262. doi:10.1016/s0092-8674(01)00456-1
28. Yang R, Xu J, Xu L, et al. Cancer cell membrane-coated adjuvant nanoparticles with mannose modification for effective anticancer vaccination. *ACS nano*. 2018;12(6):5121–5129. doi:10.1021/acsnano.7b09041
29. Kim SY, Heo MB, Hwang GS, et al. Multivalent polymer nanocomplex targeting endosomal receptor of immune cells for enhanced antitumor and systemic memory response. *Angew Chem*. 2015;54(28):8139–8143. doi:10.1002/anie.201501380
30. Yamanaka R, Honma J, Tsuchiya N, Yajima N, Kobayashi T, Tanaka R. Tumor lysate and IL-18 loaded dendritic cells elicits Th1 response, tumor-specific CD8+ cytotoxic T cells in patients with malignant glioma. *J Neuro-Oncol*. 2005;72(2):107–113. doi:10.1007/s11060-004-3550-9
31. Zamame Ramirez JA, Romagnoli GG, Falasco BF, et al. Blocking drug-induced autophagy with chloroquine in HCT-116 colon cancer cells enhances DC maturation and T cell responses induced by tumor cell lysate. *Int Immunopharmacol*. 2020;84:106495. doi:10.1016/j.intimp.2020.106495

32. Galluzzi L, Petroni G, Kroemer G. Immunogenicity of cell death driven by immune effectors. *J Immunotherap Cancer*. 2020;8(1). doi:10.1136/jitc-2020-000802
33. Zhang X, Wang C, Wang J, et al. PD-1 blockade cellular vesicles for cancer immunotherapy. *Adv Mater*. 2018;30(22):e1707112. doi:10.1002/adma.201707112
34. Lybaert L, Vlieghere ED, Rycke RD, et al. Bio-hybrid tumor cell-templated capsules: a generic formulation strategy for tumor associated antigens in view of immune therapy. *Adv Funct Mater*. 2015;24(45):7139–7150.
35. Krysko DV, Garg AD, Kaczmarek A, Krysko O, Agostinis P, Vandenabeele P. Immunogenic cell death and DAMPs in cancer therapy. *Nat Rev Cancer*. 2012;12(12):860–875. doi:10.1038/nrc3380
36. Wu Y, Li Q, Shim G, Oh YK. Melanin-loaded CpG DNA hydrogel for modulation of tumor immune microenvironment. *J Control Release*. 2021;330:540–553. doi:10.1016/j.jconrel.2020.12.040
37. Zhou F, Feng B, Yu H, et al. Tumor microenvironment-activatable prodrug vesicles for nanoenabled cancer chemoimmunotherapy combining immunogenic cell death induction and cd47 blockade. *Adv Mater*. 2019;31(14):e1805888. doi:10.1002/adma.201805888
38. Smyth MJ, Trapani JA. Granzymes: exogenous proteinases that induce target cell apoptosis. *Immunol Today*. 1995;16(4):202–206. doi:10.1016/0167-5699(95)80122-7
39. Saravia J, Chapman NM, Chi H. Helper T cell differentiation. *Cell Mol Immunol*. 2019;16(7):634–643. doi:10.1038/s41423-019-0220-6